Evolution of the Low-Frequency Spin Dynamics in Ferromagnetic Manganites

J. A. Fernandez-Baca,[1] P. Dai,[1] H. Y. Hwang,[2] C. Kloc,[2] and S-W. Cheong[2,3]
[1]*Oak Ridge National Laboratory, Oak Ridge, Tennessee 37831-6393*
[2]*Bell Laboratories, Lucent Technologies, Murray Hill, New Jersey 07974*
[3]*Department of Physics and Astronomy, Rutgers University, Piscataway, New Jersey 08855*
(Received 23 September 1997)

Neutron scattering was used to study the ferromagnetic manganites $Nd_{0.7}Sr_{0.3}MnO_3$ ($T_C = 197.9$ K) and $Pr_{0.63}Sr_{0.37}MnO_3$ ($T_C = 300.9$ K). The spin dynamical behavior of these two systems is similar at low temperatures but drastically different at temperatures around T_C. While the formation of spin clusters of size (~20 Å) dominates the spin dynamics of the 197.9 K sample close to T_C, the paramagnetic to ferromagnetic transition for the 300.9 K sample is more conventional. These results, combined with seemingly inconsistent earlier reports, reveal clear systematics in the spin dynamics of the manganites. [S0031-9007(98)06004-9]

PACS numbers: 72.15.Gd, 61.12.Ld, 75.30.Kz

The prospect of potential technological applications of the so-called colossal magnetoresistance (CMR) [1] has lead to a revival in the study of perovskite manganites $A_{1-x}B_xMnO_3$ (where A and B are trivalent and divalent ions, respectively). For compositions of $x \approx 0.3$, these materials exhibit a resistivity drop that is intimately related to the paramagnetic to ferromagnetic ordering at the Curie temperature (T_C). The magnitude of the resistivity drop and T_C can be tuned continuously by different A-site substitutions [2]. The central issue is whether the microscopic understanding of these materials is complete within the double exchange (DE) model [3] or requires additionally a strong Jahn-Teller based electron-lattice coupling [4,5]. Experimentally, large oxygen lattice distortions have been found in $La_{0.7}Ca_{0.3}MnO_3$ ($T_C \sim 250$ K) [6–8], consistent with the existence of lattice and/or magnetic polarons [9,10]. These results may also be related to the development of a prominent diffusive central peak close to T_C in this compound [11]. By contrast, no signatures of unusual oxygen lattice distortions or unconventional spin dynamics have been reported [12–14] in higher T_C materials. In particular, Perring *et al.* [13] found that the spin-wave dispersion throughout the Brillouin zone in $La_{0.7}Pb_{0.3}MnO_3$ ($T_C = 355$ K) can be described by the conventional Heisenberg ferromagnet (FM) model with only the nearest-neighbor exchange coupling. Furukawa [15] has recently shown that this result can be fully explained within the DE model.

Thus, from the current experimental evidence it is difficult to develop a consistent picture of the spin dynamical behavior in the ferromagnetic perovskite manganites. In particular, it is not known whether the central diffusive component observed in $La_{0.67}Ca_{0.33}MnO_3$ close to T_C [11] is a common feature to all CMR materials with $x \approx 0.3$. A resolution of this issue is important because a theory which purports to accurately describe the CMR effect must be able to explain the common features of all the $x \approx 0.3$ manganites.

By judicially tuning the lattice distortions through different A-site substitutions, we prepared two high quality perovskite manganite single crystals that have T_C values 197.9 K ($Nd_{0.7}Sr_{0.3}MnO_3$, or NSMO) and 300.9 K ($Pr_{0.63}Sr_{0.37}MnO_3$, or PSMO). Our aim was to study, via elastic and inelastic neutron scattering, the systematics of the unique coupling between the lattice distortion and the spin dynamics of these materials. We show that the spin dynamical behavior of these two systems is similar at low temperature, but drastically different for temperatures around T_C. While the spontaneous formation of spin clusters (~20 Å in size) close to T_C dominates the spin dynamics of the 197.7 K sample, the paramagnetic to ferromagnetic phase transition for the 300.9 K material is more conventional.

Large single crystals (≈1 cm^3) of NSMO and PSMO of mosaic spreads of ~0.5° full width at half maximum (FWHM) were grown by the floating zone method. The neutron scattering experiments were carried out using the HB-1 triple-axis spectrometer at the High-Flux Isotope Reactor at the Oak Ridge National Laboratory. We have used pyrolytic graphite (PG) as the monochromator and crystals of PG or Be as the analyzer to select neutrons with a wavelength of 2.46 Å ($E = 13.6$ meV) or 1.64 Å ($E = 30.5$ meV). The samples were slightly orthorhombic and twinned at the measured temperatures, but for the purpose of our measurements (and the utilized instrumental resolution) we assumed a cubic lattice ($a = 3.86$ Å) for both crystals.

The temperature dependence of the intensity of the (0 0 1) Bragg reflection for both samples [see Figs. 1(a) and 1(b)] indicates that ferromagnetic ordering develops at low temperatures. These measurements were done allowing sufficient time (≈20 min) for the samples to reach thermal equilibrium and were performed both on cooling (solid circles) and on warming (open circles). There is a small but reproducible hysteresis in both data sets, suggesting that the ferromagnetic phase transition is weakly first order. The difference between

 0031-9007/98/80(18)/4012(4)$15.00

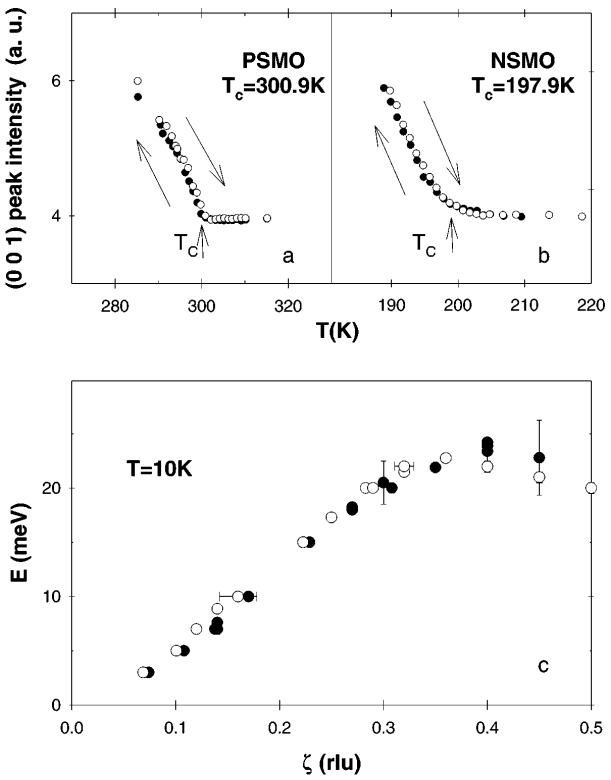

FIG. 1. Temperature dependence of the (0 0 1) Bragg reflection of (a) PSMO, and (b) NSMO on cooling (solid circles) and warming (open circles). Spin-wave dispersion curves of (c) NSMO (solid circles) and PSMO (open circles) throughout the zone $(0, 0, 1 + \zeta)$ at $T = 10$ K. The data for PSMO are from [17].

the transition temperatures on cooling and on warming was less than $\approx$0.5 K, and for the purposes of this experiment we chose the average of these two as T_C (197.9 $\pm$ 0.5 K for NSMO and 300.9 $\pm$ 0.5 K for PSMO). The ferromagnetic-to-paramagnetic transition for NSMO is significantly rounder than that for PSMO; this may be due to the special features of the former system which will be addressed below. We also note that, within the precision of our measurements, there was no evidence of spin canting [16], or of a spin diffusive peak at the antiferromagnetic positions in these two samples.

The spin-wave dispersion curve for NSMO throughout the $(0, 0, 1 + \zeta)$ Brillouin zone at 10 K is plotted in Fig. 1(c) (solid circles), which also shows similar data for PSMO (open circles) [17]. Note that despite the large difference in the T_C values of these two systems, the two curves are remarkably similar. This observation cannot be explained by any simple model of magnetic ordering. In particular, for a Heisenberg ferromagnet with only nearest-neighbor exchange interaction J, kT_C is nearly proportional to J [18]. To elucidate the nature of the spin dynamics of these two systems, we performed high-resolution neutron inelastic scattering measurements in the zone $(0, 0, 1 + \zeta)$ in the long wavelength limit (small wave vectors q). In both cases the excitation spectra consist of spin-wave peaks and a component centered at $\hbar\omega = 0$. The spin-wave peaks and the central component are well resolved up to $T = 0.98T_C$ and the spectra were least-square fitted to Gaussian line shapes. The spin-wave energies obtained from this analysis can be fitted to the well-known quadratic dispersion relation $\hbar\omega = \Delta + Dq^2$, where D is the spin-wave stiffness constant and Δ is a small dipolar gap. In the Heisenberg model, $D = 2JSa^2$, where S is the magnitude of the electronic spin at the magnetic ion sites and a is the lattice parameter. The quadratic dispersion form, however, is general and not limited to this model. In all cases a very small ($\leq$0.05 meV) energy gap was obtained from the fits, but for practical purposes this gap was assumed to be zero. To follow the spin dynamical properties closer to T_C, we show in Fig. 2 the spin-wave stiffness constant $D(T)$ vs T/T_C for both samples up to $T/T_C = 0.98$. As $T \rightarrow T_C$, the hydrodynamic and the mode-mode coupling theories [19] predict a temperature dependence of the spin-wave stiffness of the form $D(T) \sim [(T - T_C)/T_C]^{\nu-\beta}$. The fit of the spin-wave data for PSMO to this form yields an exponent $(\nu - \beta) \approx 0.38 \pm 0.05$ (solid line in Fig. 2). This exponent should be compared to the value 0.34 predicted for a Heisenberg FM and to the measured values for iron (0.36 $\pm$ 0.03), cobalt (0.39 $\pm$ 0.05) or nickel (0.39 $\pm$ 0.04) [19]. The data for NSMO, on the other hand, show no evidence of the expected spin-wave collapse at T_C, just as in $La_{0.67}Ca_{0.33}MnO_3$ [11]. Thus, while the low-temperature spin-wave stiffness for PSMO and NSMO is $D(0) \approx 165$ meV Å^2 (very similar to the 170 meV Å^2 for $La_{0.67}Ca_{0.33}MnO_3$), it is evident that the

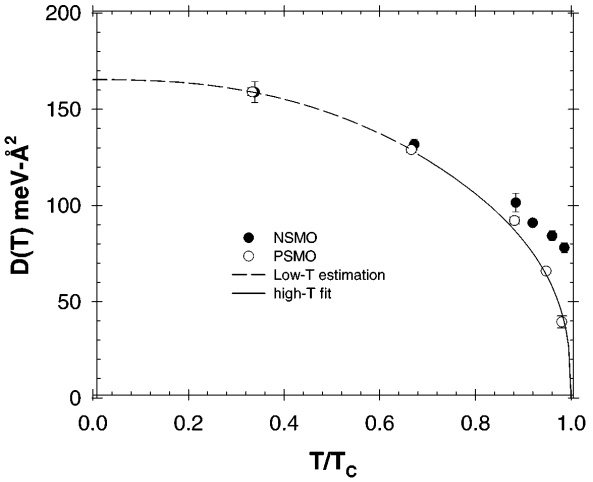

FIG. 2. Spin-wave stiffness $D(T)$ vs T/T_C for PSMO (open circles) and NSMO (solid circles). The solid line is the fit to the mode-mode coupling and hydrodynamic theories at high temperatures. The dashed line is an extrapolation to $T = 0$ from the low-temperature mode-mode coupling theory [i.e., $D(T) = D(0)(1 - AT^{5/2})$].

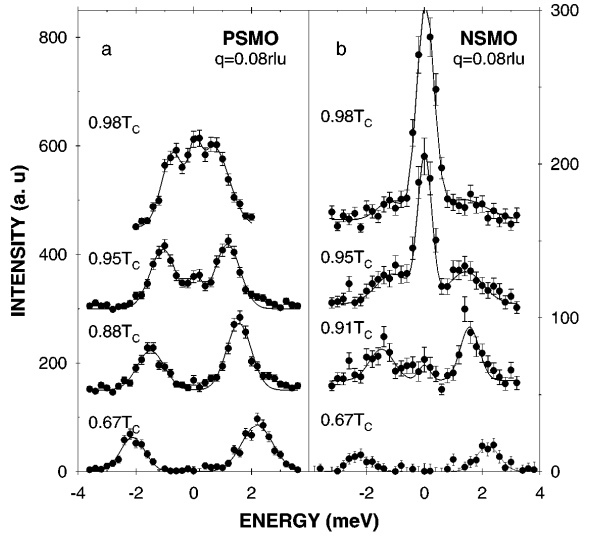

FIG. 3. Energy scans for (a) PSMO, and (b) NSMO at $q = 0.08$ rlu.

spin dynamics of these two systems become different as $T \rightarrow T_C$.

The striking differences between the spin-dynamical behavior of PSMO and NSMO as $T \rightarrow T_C$ are illustrated in Fig. 3. This figure shows energy (constant-q) scans for an arbitrary wave vector $q = 0.8$ reciprocal lattice units (rlu). The peaks at the positive side of the energy axis correspond to neutron energy loss while those at the negative side are for neutron energy gain. A weak nonmagnetic elastic incoherent contribution at $\hbar\omega = 0$ has been subtracted. Both data sets show spin-wave excitations of similar energies at the lower temperatures and these energies decrease as the temperature is increased. In PSMO [Fig. 3(a)], the excitations soften and become more intense as $T \rightarrow T_C$ as expected for a conventional FM. With increasing temperature, a central component develops. This central peak may be related to the longitudinal spin fluctuations from a Heisenberg FM at high temperatures, where the spin-wave description is not strictly valid [20], or it may already be a precursor of the spin dynamics seen in the lower T_C NSMO, which is definitely unconventional. Above $\approx 0.91T_C$, the spin-wave energy renormalization in NSMO is slower than in PSMO, while the spin-wave intensities damp dramatically and the excitation spectrum is dominated by the central component [21]. Figure 4 shows a plot of the intensity of this component (normalized by the spin-wave intensity at $T = 0.66T_C$) vs T/T_C for both systems. The temperature dependence of the central component shown in Fig. 4 is somewhat different from that reported for $La_{0.67}Ca_{0.33}MnO_3$[11], which starts to develop above $T \approx 0.6T_C$. The intrinsic width Γ of the central component in NSMO follows the quadratic dependence in q expected for spin diffusion (i.e., $\Gamma = \Lambda q^2$); the inset of Fig. 4 shows the FWHM linewidth Γ vs q^2 at $T = 0.98T_C$ ($\Lambda = 26(2)$ meV Å^2). This diffusive component persists

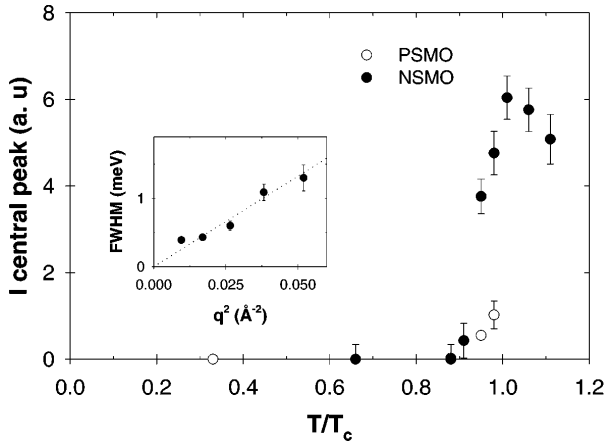

FIG. 4. Temperature dependence of the intensity of the central component in PSMO and NSMO. The inset shows the FWHM linewidth of this component for NSMO vs q^2.

at least up to $T = 1.25T_C$ with little T dependence above T_C. The magnetic nature of this component was verified by performing measurements close to the (0 0 2) Brillouin zone center which showed the expected intensity drop due to the Mn magnetic form factor.

To characterize the nature of the diffusive component of both samples, we performed systematic measurements of

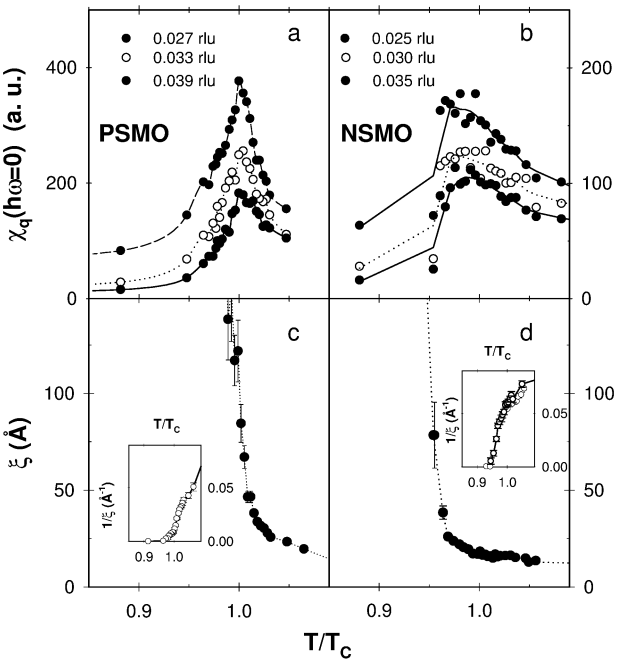

FIG. 5. (a) Temperature dependence of the static wave-vector-dependent susceptibility $\chi_{\mathbf{q}}(\hbar\omega = 0)$ for PSMO. (b) $\chi_{\mathbf{q}}(\hbar\omega = 0)$ for NSMO. These measurements were performed with an energy window of 0.43 meV (this is the FWHM energy resolution at the elastic position of the experimental setup). Temperature dependence of the spin-correlation length for (c) PSMO and (d) NSMO. Insets: temperature dependence of the inverse spin-correlation length.

TABLE I. Summary of magnetic properties of various perovskite manganites $A_{1-x}B_xMnO_3$ ($x \approx 0.3$) in order of decreasing T_C.

Manganite	T_C (K)	$D(0)$ (meV Å^2)	$\frac{D(0)}{kT_C}$ (Å^2)
$La_{0.7}Sr_{0.3}MnO_3$, Ref. [12]	378	188	5.8
$La_{0.7}Pb_{0.3}MnO_3$, Ref. [13]	355	134	4.4
$Pr_{0.63}Sr_{0.37}MnO_3$, this work	300.9	165	6.4
$La_{0.67}Ca_{0.33}MnO_3$, Ref. [11]	250	170	7.9
$Nd_{0.7}Sr_{0.3}MnO_3$, this work	197.9	165	9.7

the static wave-vector-dependent susceptibility $\chi_{\mathbf{q}}(\hbar\omega = 0)$, and the static spin-correlation function. These were "elastic" neutron scattering measurements performed with and without energy analysis [19,20]. The temperature dependence of $\chi_{\mathbf{q}}(\hbar\omega = 0)$ is shown in Figs. 5(a) and 5(b) for several selected wave vectors. For PSMO the susceptibility shows a sharp peak at the FM transition, as expected for a conventional FM, while the data for NSMO exhibits a broad peak with a maximum at a temperature below T_C. The profiles of the measured static spin-correlation function were least-squared fitted to an Ornstein-Zernike cross section [19] convoluted with the instrumental resolution. From these fits we obtained $\kappa(T) = 1/\xi(T)$, where $\xi(T)$ is the spin-correlation length. Figures 5(c) and 5(d) show the temperature dependence of the spin-correlation length ξ, and the insets show the corresponding temperature dependence of $\kappa(T)$ for both systems. For PSMO, the spin-correlation length $\xi(T)$ increases on cooling and diverges [$\xi(T) > 100$ Å] close to T_C, indicating the onset of long-range FM order. In contrast, the spin-correlation length ξ for NSMO is relatively insensitive to T and remains small ($\approx$20 Å) at T_C. $\xi(T)$ grows to over 100 Å only at $T \approx 0.95T_C$. This result is different from that of Ref. [9], which suggests that $\xi(T)$ diverges at T_C for LCMO.

Our results clearly demonstrate that while the magnetism of these two ferromagnetic manganites in the low-temperature metallic state may be similar, their spin dynamical behavior around T_C can be drastically different. Therefore, it becomes clear that magnetism alone cannot explain the exotic spin dynamical properties in these systems and that the increased electron-lattice coupling plays a dominant role. In Table I we emphasize this point by summarizing the results of our experiments as well as those for other perovskite manganites $A_{1-x}B_xMnO_3$ ($x \approx 0.3$). This table has been organized in order of decreasing T_C. For the three highest T_C systems, the values of $D(0)/kT_C$ are characteristic of typical localized ferromagnets. Larger $D(0)/kT_C$ values, more characteristic of itinerant ferromagnets [22], are observed in the last two (lower T_C) systems. This systematic trend occurs despite the fact that with decreasing T_C, the zero temperature insulating state is approached.

We are grateful to D. Belanger, J. W. Cable, J. F. Cooke, J. W. Lynn, H. A. Mook, S. E. Nagler, R. M. Moon, D. A. Tenant, and H. Yoshizawa for helpful discussions. We acknowledge the expert technical support provided to us by R. G. Maples, S. Moore, and G. B. Taylor. ORNL is managed by Lockheed Martin Energy Research Corp. for the U.S. DOE under Contract No. DE-AC05-96OR22464.

[1] S. Jin *et al.,* Science **264**, 413 (1994).
[2] H. Y. Hwang *et al.,* Phys. Rev. Lett. **75**, 914 (1995).
[3] C. Zener, Phys. Rev. **82**, 403 (1951); P. W. Anderson and H. Hasegawa, *ibid.* **100**, 675 (1955).
[4] A. J. Millis *et al.,* Phys. Rev. Lett. **74**, 5144 (1995); **77**, 175 (1996).
[5] H. Röder, Jun Zang, and A. R. Bishop, Phys. Rev. Lett. **76**, 1356 (1996).
[6] P. Dai *et al.,* Phys. Rev. B **54**, R3694 (1996).
[7] P. G. Radaelli *et al.,* Phys. Rev. B **54**, 8992 (1996).
[8] S. J. L. Billinge *et al.,* Phys. Rev. Lett. **77**, 715 (1996).
[9] J. M. de Teresa *et al.,* Nature (London) **386**, 256 (1997).
[10] R. W. Erwin *et al.,* J. Appl. Phys. **81**, 5487 (1997).
[11] J. W. Lynn *et al.,* Phys. Rev. Lett. **76**, 4046 (1996).
[12] M. Martin *et al.,* Phys. Rev. B **53**, R14 285 (1996).
[13] T. G. Perring *et al.,* Phys. Rev. Lett. **77**, 711 (1996).
[14] Y. Endoh and K. Hirota, J. Phys. Soc. Jpn. **66**, 2264 (1997).
[15] N. Furukawa, J. Phys. Soc. Jpn. **65**, 1174 (1996).
[16] P. G. DeGennes, Phys. Rev. **118**, 141 (1960).
[17] H. Y. Hwang *et al.,* Phys. Rev. Lett. **80**, 1316 (1998).
[18] G. S. Rushbrooke *et al.,* in *Phase Transitions and Critical Phenomena,* edited by C. Domb and M. S. Green (Academic, New York, 1974).
[19] M. Collins in *Magnetic Critical Scattering* (Clarendon, Oxford, 1989).
[20] S. Lovesey in *Theory of Thermal Neutron Scattering from Condensed Matter* (Clarendon, Oxford, 1984), Vol. 2.
[21] The crystalline electric field levels in Nd^{3+} in a cubic lattice consist of one doublet and three quartets. At all temperatures there is quasielastic scattering from transitions within these magnetic multiplets, which can have a contribution to the temperature evolution of the central peak in NSMO. We have determined that this contribution should increase smoothly with temperature and, therefore, cannot account for the rather abrupt increase of the central component observed in NSMO above $0.91T_C$ (see Fig. 4).
[22] H. A. Mook, in *Spin Waves and Magnetic Excitations I,* edited by A. S. Borovik-Romanov and S. K. Sinha (Elsevier, Amsterdam, 1988), p. 444.